

FUNDAMENTALS OF ABSOLUTE PYRHELIOMETRY

AND OBJECTIVE CHARACTERIZATION

D. A. Crommelynck  
Royal Meteorological Institute  
Brussels, Belgium

INTRODUCTION: ABSOLUTE INSTRUMENTS FOR IRRADIANCE MEASUREMENTS

The accurate measurement of the irradiance on a given surface is not trivial. It is the purpose of this contribution to describe the radiometric methodology in use at the Royal Meteorological Institute (RMI) and to show the importance of radiometer characterizations.

As an example, we will consider the narrow-field-of-view radiometer developed at the RMI for the observation of the solar constant. The metrology of radiation is a difficult subject which is strongly dependent on the radiation source behavior. The radiation field will seldom be distributed uniformly. Generally the space-time variability of natural radiation fields is large. For our purpose, to simplify the problem, we will consider the Sun's radiation output to be constant. The solar source can be monitored by a single instrument accurately pointed at the Sun, to measure its output as a function of time. In this simplest case, we will show how it is possible to perform absolute measurements with relatively high accuracy.

An instrument can be considered to be absolute if its measurements expressed in SI units are based only on the independent knowledge of the different coefficients appearing in the equation defining the output signal in terms of basic physical characteristics. An absolute radiometer may thus in no case be calibrated by comparison to another radiometer. The purpose of radiometric comparisons of absolute radiometers is only to measure the differences found between different and independent technologies. These differences, if sufficiently small, are an indication of the state of the art.

ANGULAR RESPONSE OF RADIOMETER

Absolute radiometer detectors are usually built without any optical accessories such as lenses or mirrors, because these would introduce nonuniformities in spectral sensitivity. The sensors are generally designed to have the highest effective efficiency for radiation sensing, and their sensitive area is determined by the area of a hole placed in front of the cavity of the detector at the sensor plane (fig. 1). (See the section on cavity sensor efficiency.) If the hole is circular, an ideal behavior is a cosine response to the displacement of a point source  $s$  in a plane passing at  $n$  with a constant  $S_s$  distance and a variable incident angle  $Z_i$ , as long as  $s$  is in the full light zone. The sensor responds to all sources in the CDsAB hemisphere (shown in fig. 1), which includes the field-of-view (FOV) limiting device. However, the FOV limiter is

meant to provide a shadow zone where the source  $s$  cannot be seen by the sensor. When the source is in the penumbra zone the response is proportional to the part of the sensitive area which is irradiated.

The geometric characteristics of the radiometer are thus essentially fixed by the limit angle  $Z_1$  and the slope angle  $Z_p$ , which are functions of the distance  $l$  between the front aperture plane and the sensor plane. The front aperture (radius  $R$ ) is centered on the sensitive area of the sensor (radius  $r$ ). Thus

$$Z_1 = \arctan (R + r)/l \quad (1a)$$

$$Z_p = \arctan (R - r)/l \quad (1b)$$

A general analysis and computation of the radiometric angular response is given by Kendall (1978).

#### ABSOLUTE DETECTOR

The absolute measurement of radiative energy is done ideally by comparison with electrical energy; both energy forms induce thermal fields which can be compared if their initial and boundary conditions are identical. The measurement of the temperature at well-defined points of the fields is not easily done with identical heat losses. It is more appropriate to compare the heat transfer of the fields to a common heat sink, since the sensitivity of the measurement is then higher and the physical definition of the heat loss path is better.

The comparison is essentially based on the ability either to transform the two different energies completely into heat, or, if this is not possible, to know accurately the effective absorption coefficient of the surface exposed to the radiation. In fact, the absolute detector will thus have an absorbing sensitive surface on which an electric heater is built. The heat flux is conducted through a well-defined path towards a thermal heat sink and is then measured.

An absolute radiometer sensor can be assembled in a certain number of ways, depending on the type of absorbing surface. This in turn dictates the use of a certain heater and heat flux sensor. The sensitive surface can simply be painted black and can be provided with an optical feedback mirror to enhance the effective absorption of the surface (A in fig. 2). Alternatively, the interior of the cavity can be coated with a diffuse black paint, or it can have a specular surface. The selection of the surface depends on the shape of the cavity, which can be cylindrical with a flat bottom or upwards or downwards conical. The heating element will similarly be flat, cylindrical, or conical. The heat flux detector can be based on a thermoelectric or a thermoresistive method. These detectors can be in the shape of a star or a full or hollow disk.

Several possible combinations of cavities, sensors, and heaters are shown in figure 2; working examples include the Crom radiometer (B-II-b), the active cavity radiometer (C-IV-d), and the PMO (Physical Meteorological Observatory) radiometer with thermoresistive sensors and an inverted cone (D-III-d). The combinations C-III-d and A-II-b were tested at the Royal Meteorological Institute,

B-I-c and B-I-b were tested at the National Bureau of Standards, and I-b was tested at the National Physical Laboratory.

A good knowledge of the characteristics of these elements is required. One such characteristic is the sensitivity of the heat flux sensor, which is a function of temperature, output resistance, and thermal conductivity. For the cavity, the absorption of the paint and the resulting effective absorption of the cavity, the emissivity of the outer wall, and the thermal conductivity of its material must be known. It is necessary to be able to monitor the heating part of the resistance heater; this means that it should be fed by a four-wire setup.

Since thermal detectors present a response time, and since the temperature of the heat sink is not fixed at a preset value, thermal compensation must be built into the sensor. This is accomplished by using a differential technique consisting of two sensors, either or both of which are irradiable. The second sensor should be as identical as possible to the first and should also be provided with a heating resistor. If the sensors are placed side by side and either one can be irradiated, the detector is described as being dual compensated; if the second sensor cannot be irradiated then the detector is described as being compensated.

#### PRINCIPLES FOR ABSOLUTE RADIOMETRIC MEASUREMENTS

Compensated or dual-compensated absolute detectors can generally be used either passively, by directly measuring the output of the thermal detector in response to radiative input, or with the support of an active electronic feedback system. (Refer to the section on active modes of operation.) In both cases the radiometer must be calibrated electrically with a calibration source that duplicates the radiation fields to be measured. In the first case this is done manually, usually before and after a period of 20 minutes of radiation measurements. In the second case, channel open and closed states follow each other every 90 seconds, and the irradiance is given by a relation of the form

$$\Phi = K(P_C - P_O) \quad (2)$$

where  $P_C$  is the electrical power sent to the detector when the detector is closed and  $P_O$  is the electrical power sent to the detector when the detector is exposed to the radiation. The value of  $K$  depends on the sensitive area of the detector and its efficiency. The active mode of operation gives a faster time response from the radiometric system than is possible without feedback electronics. (See the section on frequency response of heat flux detector and absolute radiometer system.)

The dual-channel active-cavity radiometers developed by the author at the Royal Meteorological Institute can be operated as described. (See equations (35) through (39).) However, since the second compensating channel is exactly the same as the measuring channel, and since they are fixed next to each other with their axes parallel and pointing in the same direction, it is also possible to operate this radiometer in the Angström mode, by directly and

simultaneously comparing the radiative energy and the electrical energy. This is done by measuring the thermoelectric signal difference between the detectors. This very versatile mode of operation of the dual-channel active-cavity absolute radiometer makes it possible to perform consistency tests between channels and measuring methods.

#### ACTIVE MODES OF OPERATION

An absolute radiometer used in an active measurement mode can be set up in several ways, depending on whether the feedback electrical power is reinjected at the irradiated heat flux detector or at the nonirradiated compensation side. The type of setup also depends on whether the signal coming from the detector is compared to a reference voltage or to the signal obtained at the output of the compensation detector excited by a reference electrical source. In principle, the same feedback electronics are used in each case. These consist of an error amplifier followed by an ad hoc PDI (proportional differential integrator) system and then an inverter, the whole of which is represented by the block transfer function  $H_a(f)$ . This is followed by a square root function to linearize the system and an output amplifier of transfer function  $H_c(f)$  (fig. 3).

The measurement depends in each case on the knowledge of the compensation current  $I_c$ , which is measured by the voltage induced in the reference resistance  $R_M$ . The error signal  $\Delta V$  is the difference between the output signal of the operating channel of the radiometer and the reference channel  $V_{12p}$  (figs. 3(a) and 3(d)),  $F$  (fig. 3(b)), or  $V_{12p} + F$  (fig. 3(c)). The heating resistors are represented by  $R_1$  and  $R_2$ , respectively, for the first and second detector,  $\alpha_1$  is the optical efficiency of detector  $D_1$ , and  $G_1$  and  $G_2$  are the ratios of the output signal of the first or second detector, respectively, to the electrical excitation  $P_1$  or  $P_2$ . Each case is considered separately; thus it is easy to calculate  $I_c$  as a function of the incident flux  $\phi_1$  at steady state.

For a double-compensated radiometer (fig. 3(a)), the irradiated sensor is not in the servo loop, and as a result the ratio  $G_2/G_1$  needs to be accurately known, as do  $R_2$  and  $\alpha_1$ , as shown by the relation

$$\phi_1 = \frac{G_2}{G_1} \frac{I_c^2 R_2}{\alpha_1} \left[ \frac{(R_2 + R_M)^2}{R_2 G_2 H_a H_c^2} + 1 \right] \quad (3)$$

where for an accurate servo system the bracketed expression tends to be equal to 1. With this setup appropriately and successively inverted from the first to the second detector it is possible to operate in the Angström mode, as described previously. The calculated flux will be either the arithmetic or the geometric mean of two successive observations. This allows the elimination of the ratio  $G_2/G_1$  from equation (3) at steady state.

In the case of a thermally uncompensated single radiometer (fig. 3(b)), some parasitic thermal effects are not removed from the measurements. As shown by the relation

$$\phi_1 = \frac{R_1 I_C^2}{\alpha_1} \left[ \frac{(R_1 + R_M)^2}{R_1 G_1 H_a H_C^2} - 1 \right] + \frac{F}{\alpha_1 G_1} - \frac{V_{110}}{\alpha_1 G_1} \quad (4)$$

some residual thermoelectric offset ( $V_{110}$ ) can perturb the instrument when not irradiated. The measurement of the incident flux should be obtained by successive open and closed measurements, the latter being zero checks.

The setup shown in figure 3(c) is an improvement compared to that in figure 3(b); however, the compensation detector does not work at the same excitation level as the irradiated detector. The corresponding radiometric equation

$$\phi_1 = \frac{R_1 I_C^2}{\alpha_1} \left[ \frac{(R_1 + R_M)^2}{R_1 G_1 H_a H_C^2} - 1 \right] + \frac{F}{\alpha_1 G_1} + (V_{120} - V_{110}) \frac{1}{\alpha_1 G_1} \quad (5)$$

shows that the parasitic thermoelectric effect will be decreased.

The most commonly used system works with the irradiated and compensated detectors at the same power level (fig. 3(d)). As in the setups shown in figures 3(b) and 3(c), the irradiated detector is included in the servo loop and the system thus has a relatively fast time response. As shown by the corresponding radiometric equation

$$\phi_1 = \frac{I_C^2 R_1}{\alpha_1} \left[ \frac{(R_1 + R_M)^2}{R_1 G_1 H_a H_C^2} - 1 \right] + I_2^2 \frac{R_2 G_2}{\alpha_1 G_1} \quad (6)$$

the offset power  $I_2^2 R_2 (G_2 / \alpha_1 G_1)$  must be removed from the final equation by the execution of successive open and closed measurements, during which the offset is to be held constant. The difference between two successive open and closed states:

$$\text{Closed: } \phi'_\rho = \frac{P_c}{\alpha_1} \left[ \frac{(R_1 + R_M)^2}{R_1 G_1 H_a H_C^2} - 1 \right] + I_2^2 \frac{R_2 G_2}{\alpha_1 G_1} \quad (7a)$$

$$\text{Open: } \phi_1 + \phi_\rho = \frac{P_o}{\alpha_1} \left[ \frac{(R_1 + R_M)^2}{R_1 G_1 H_a H_C^2} - 1 \right] + I_2^2 \frac{R_2 G_2}{\alpha_1 G_1} \quad (7b)$$

gives the incident radiation flux  $\Phi$ :

$$\Phi_1 = \frac{P_O - P_C}{\alpha_1} \left[ \frac{(R_1 + R_M)^2}{R_1 G_1 H_a H_c^2} - 1 \right] \quad (8)$$

assuming the difference  $(\Phi_\rho - \Phi'_\rho)$  is negligible.

#### INSTRUMENTAL PERTURBATIONS AND SENSOR EFFICIENCY

If the radiometer responded only to the radiation incident on the sensitive area of the sensor and coming only from the observed source, then the accuracy of the measurement would depend only on the knowledge of the sensor's efficiency. This is, in fact, not the case, due to a series of parasitic effects which must be taken into account in the radiometric equation (fig. 4).

In a dual-channel absolute radiometer measuring in the successive mode operation, account must be taken of the residual dissymmetry between the two channels during the open state. This dissymmetry is due to

The effect of radiation arriving from outside and incident on the separation plane of the sensor but not on the sensitive area; this induces direct thermal effects  $\Phi_\tau$  between the separation plane and the sensor due to conductive and convective exchanges, with  $\tau = \Phi_\tau/\Phi$

Parasitic scattered radiation  $\Phi_\Sigma$  on the sensor area coming from the inside of the front field limiter through (a) reflection on the separation plane or (b) incidence from a source outside the limit angle, where  $\Sigma = \Phi_\Sigma/\Phi$

Unwanted radiation scattered and diffracted on the front aperture ( $\Phi_{\Sigma'}, \Phi_\delta$ ) with  $\Sigma' = \Phi_{\Sigma'}/\Phi$  and  $\delta = \Phi_\delta/\Phi$

The effect of front aperture heating  $\Phi_\psi$  with  $\psi = \Phi_\psi/\Phi$

The difference in infrared energy radiated by the front aperture system to the two channels

These effects are conveniently expressed as a function of the flux  $\Phi$  incident on the sensitive area. The sensor's efficiency depends on the geometry of the cavity and its coating as well as on the way the heat current is conducted to the heat flux detector.

In the particular case of the absolute instrument developed at the Royal Meteorological Institute the cavity is cylindrical, with a flat bottom covered on the inside with a diffusing black paint. The outside of the cavity's silver

wall is polished and gold-plated. The bottom is in direct thermal contact with the heat flux detector. In this way the radiation which falls directly on the bottom is absorbed and measured according to the absorption coefficient  $a_p$  of the paint. The reflected radiation  $(1 - a_p)$  falling on the cylindrical wall is a function of the diffusion pattern of the paint, which is considered by the paint manufacturer to be Lambertian. To calculate the total efficiency of the detector, the relative sensitivity distribution of the cylindrical cavity must be known.

Finally, thermal expansion of the sensor's sensitive area must also be taken into account. Some of the resulting effects can be calculated on the basis of fairly acceptable assumptions; however, for most of the effects an actual physical characterization is necessary because modeling is not always sufficiently representative of reality. These characterization experiments should be feasible on every absolute radiometer.

#### HEATING WIRE EFFECT

The accuracy of the absolute radiometric measurements depends on the precise physical definition of the elements whose values appear in the radiometric equation. One of these elements is the value of the compensating heating resistance. This value  $R_i$ , as well as the power  $P_i$  which is dissipated, is obtained by direct and simultaneous measurement of the heater current  $I_i$  and the applied voltage  $U_i$ . This can be done with a high degree of electrical accuracy; however, it is possible that the heating wires  $cd$  and  $c'd'$  contribute to some parasitic electrical power dissipation detected by the heat flux detectors, which in turn could give rise to some systematic error (fig. 5).

Let us assume that the measured parasitic powers  $P_{p1}$  and  $P_{p2}$  are due to the equivalent parasitic heaters  $r_c$ ,  $r_d$ ,  $r_{c'}$ , and  $r_{d'}$ . Electrical heating can therefore be expressed by

$$V_{11P} = G_1(r_c + R_1 + r_d)I_1^2 = G_1R_1I_1^2 + G_1P_{p1} \quad (9a)$$

and

$$V_{12P} = G_2(r_{c'} + R_2 + r_{d'})I_2^2 = G_2R_2I_2^2 + G_2P_{p2} \quad (9b)$$

where  $G_1$  and  $G_2$  are trimmed by  $p1$  and  $p2$  such that when  $R_1I_1^2 = R_2I_2^2$  with  $R_1 = U_1/I_1$  and  $R_2 = U_2/I_2$  we have

$$\Delta V = V_{11P} - V_{12P} = 0 \quad (10)$$

At this point we can define  $G_1' = V_{11P}/R_1 I_1^2$  and  $G_2' = V_{12P}/R_2 I_2^2$  where  $G_1' \rightarrow G_1$  and  $G_2' \rightarrow G_2$  when the parasitic heating effects tend to zero. The easiest way to determine the parasitic effect is to inject successively the currents  $I_{1c} = I_{1d} = I_1$  and  $I_{1c'} = I_{1d'} = I_2$  in the respective wires (cAa, dBb) and (c'A'a', d'B'b') and detect the corresponding  $V_{11P}$  and  $V_{12P}$  deviations. Here the hypothesis is made, based on symmetry, that  $r_a = r_c$ ,  $r_d = r_b$ ,  $r_{a'} = r_{c'}$ , and  $r_{d'} = r_{b'}$ . Therefore we find that

$$r_c = \frac{V_{11Pc}}{2G_1' I_{1c}^2} \quad (11a)$$

$$r_d = \frac{V_{11Pd}}{2G_1' I_{1d}^2} \quad (11b)$$

$$r_{c'} = \frac{V_{12Pc'}}{2G_2' I_{2c'}^2} \quad (11c)$$

$$r_{d'} = \frac{V_{12Pd'}}{2G_2' I_{2d'}^2} \quad (11d)$$

where  $G_1$  and  $G_2$  are approximated by  $G_1'$  and  $G_2'$ . The effective heating is thus equal to the measured heating  $R_1 I_1^2$  or  $R_2 I_2^2$  plus the parasitic effects  $(r_c + r_d) I_1^2$  or  $(r_{c'} + r_{d'}) I_2^2$ .

If this is applied to absolute radiometric measurements based on successive open and closed states of the irradiated channel 1 of a dual-channel active absolute radiometer, we find, if the excitation of the reference channel is kept constant, that

$$\begin{aligned} \Phi = K(P_c - P_o) &= K \left[ R_1 I_{1c}^2 + (r_c + r_d) I_{1c}^2 - R_1 I_{10}^2 - (r_c + r_d) I_{10}^2 \right] \\ &= K \left[ R_1 (I_{1c}^2 - I_{10}^2) + (r_c + r_d) (I_{1c}^2 - I_{10}^2) \right] \end{aligned} \quad (12)$$

where  $K(r_c + r_d) (I_{1c}^2 - I_{10}^2)$  is the error due to the parasitic heating effect.

CAVITY SENSOR EFFICIENCY

Due to the thermal configuration of the cavity sensor as well as the reflection pattern of its inner coating, this sensor is not of uniform sensitivity. The heat flux meter output is proportional to

$$\int_{\lambda} \int_{\text{Cavity}} a(\lambda, r) \Phi(\lambda, r) dr d\lambda = K_1 V_1 \Phi \quad (13)$$

In fact,  $\Phi(\lambda, r) = \Phi(\lambda)$  is uniform over the direct irradiated sensor cavity bottom; elsewhere, for instance on the wall of the cylinder, the distribution depends on the reflected radiation. (See fig. 6.) Since we desire to measure the value of the irradiance  $E$  incident on the sensor, and since the heat flux meter deviates proportionally to the input, we need to know  $a(\lambda, r)$ . We first assume separability at the first order; thus,  $a(\lambda, r) = a'(\lambda)a'(r)$ . Let us also assume that  $\Phi(\lambda, r)$  contains the different parasitic effects considered in the discussion on instrument perturbations. Thus

$$\Phi = \int_{\lambda} \int_S \Phi(\lambda) dr d\lambda = ES + \Phi_{\psi} + \Phi_{\Sigma'} + \Phi_{\Sigma} + \Phi_{\delta} + \Phi_{\tau} - \Phi_R + \Phi_{\rho} \quad (14)$$

The energy budget of the sensor can then be written for radiative input:

$$\begin{aligned} ES \left[ 1 + \psi + \Sigma' + \Sigma + \delta + \tau - (1 - a_R) + \rho \right] \\ = K_2 \int_{\lambda} \int_{\text{Cavity}} a(\lambda, r) \Phi(\lambda, r) d\lambda dr + L + \Phi_E \end{aligned} \quad (15)$$

where  $L$  represents all thermal losses except those coming from the sensor area itself. For the latter, we consider  $\Phi_R$  to be the radiation reflected by the cavity, and  $\Phi_E$  to be the energy emitted by the cavity. In fact,  $\Phi_R = (1 - a_R)ES$  where  $a_R$  is the effective absorption coefficient of the cavity. (See the section on cavity sensor effective absorption coefficient.) In a similar way, we have for electrical energy input:

$$P = IU = \int_{\text{Cavity}} P(r) dr + L' + \Phi_E' = K_3 V_1 P \quad (16)$$

where  $L'$  represents all the thermal losses in the cavity when the sensor is electrically excited, and  $\Phi_E'$  is the energy emitted by the cavity in the same circumstances. In fact, when

$$\int_{\lambda} \int_{\text{Cavity}} a(\lambda, r) \Phi(\lambda, r) dr d\lambda = P \quad (17)$$

we have  $K_1 V_1 \Phi = K_3 V_1 P$  and thus also  $\Phi = K_2 P + L + \Phi_E$ . With this formula it is necessary to know  $K_2$ ,  $L$ , and  $\Phi_E$ . However, equation (17) can be decomposed into

$$\int_{\lambda} \int_{\text{Bottom}} a(\lambda, r) \Phi(\lambda) dr d\lambda + \int_{\text{Wall}} a(\lambda, z) \Phi(\lambda, z) dz d\lambda = P \quad (18)$$

where  $z$  is the height above the bottom of the cylinder.

If  $a'(\lambda) = a_{514}$  (see the section on spectral sensitivity of the absolute sensor), and if we assume  $a'(r) = 1$  (this assumes uniform sensitivity of the bottom of the cavity), we have

$$a_{514} \int_{\lambda} \int_S \Phi(\lambda) dr d\lambda + a_{514} \int_{\lambda} \int_z \alpha(z) \Phi(\lambda, z) dz d\lambda = P \quad (19)$$

Since

$$\Phi(\lambda, z) = (1 - a_{514}) d(z) \int_{\lambda} \int_S \Phi(\lambda) dr d\lambda \quad (20)$$

we find that

$$a_{514} \Phi + a_{514} (1 - a_{514}) \Phi \int_z \alpha(z) d(z) dz = P \quad (21)$$

With  $m(z) = \alpha(z) d(z)$  we have finally

$$\Phi a_{514} \left[ 1 + (1 - a_{514}) \int_z m(z) dz \right] = P \quad (22)$$

The factor

$$a_{514} \left[ 1 + (1 - a_{514}) \int_z m(z) dz \right] = \alpha_{\text{eff}} = P/\Phi \quad (23)$$

is the efficiency factor of the sensor where

- $d(z)$  relative radiation distribution function of the radiative energy reflected from the bottom of the cavity towards the wall of the cylinder band
- $\alpha(z)$  relative efficiency function along the wall surface of the cylinder, i.e., the electrical power needed to balance the effect of an incident laser beam kept at constant amplitude and scanning the wall of the cylinder
- $m(z)$  relative efficiency function of the tube

As a first good approximation,  $a_{514}$  is the value of the absorption factor of the black paint at  $\lambda = 514$  nm; however, this value should be very slightly increased due to the fact that the wall of the tube does not totally absorb the incident radiation and reflects part of it back to the bottom (fig. 7). When an error calculation is made to determine the effect of the uncertainty of the absorption coefficient of the paint and the effect of the tube, it will be seen that accuracy can be improved by approximately an order of magnitude by using a cavity element.

#### Cavity Sensor Relative Efficiency Distribution

The experimental determination of the relative surface efficiency distribution of the cavity sensor  $\alpha(z)$  is done with a laser beam (figs. 8 and 9). The measurements are made in air and in a vacuum. In the first phase the laser beam is normally incident on the bottom of the cavity and is moved stepwise from left to right and back. The response of the radiometer is measured with its own electronics.

In air the sensitivity variation over one diameter is at maximum  $7 \times 10^{-4}$  with a signal variability of the same value. In a vacuum, the highest observed relative difference is  $2.8 \times 10^{-4}$  with a variability of  $2 \times 10^{-4}$ . Therefore, we can only say that the sensitivity uniformity is certainly better than  $2.8 \times 10^{-4}$  and that convection effects introduce noise into the experiment in air.

In the second phase the cavity is tilted  $6^\circ$ , and the laser beam is now moved to scan first a part of the bottom and then the vertical wall of the cylindrical cavity. Although the shape of the projection of the beam is not ideal, the resulting observations (fig. 7) show clearly that the efficiency of the cylindrical cavity is better in a vacuum than in air. This is due to the removal of the convection losses. The residual losses should be attributed mainly to losses through the sensor-sensitive area, with some second-order radiative losses between the outer side of the cylinder and the surroundings.

## Cavity Sensor Effective Absorption Coefficient

The cavity sensor effective absorption coefficient  $a_R$  can be evaluated according to the geometry of the cylindrical cavity and the absorption coefficient  $a$  of its inner coating. Since the length to reduced radius ratio is 15 and since  $a = 0.97 \pm 0.01$ , we have  $a_R = 0.99986$ . (Without the sensor entrance field stop this length is 8, and then  $a_R = 0.99898$ .)

It is useful to measure  $a_R$  directly to be able to cross-check the theory, and also to try to ascertain the accuracy to which  $a_R$  can be determined. We made this determination by using a conical reflectometer developed at the World Radiation Center in Davos. The experimental setup is shown in figure 10. A laser beam is chopped, and a synchronous amplifier is used to detect the output signal of the reflectometer proportional to the back-reflected radiation of the cavity. When sufficient care is taken to avoid mechanical and background noise picked up by the conical pyroelectrical detector, it is possible to observe a reflectivity of 0.00025 with a repetition dispersion of  $\pm 0.00003$ . The value of  $a_R$  is given by the ratio

$$a_R = \frac{(S_C - S_{Cl}) - (S_{RC} - S_{Cl})}{[(S_W - S_{Cl}) - (S_{RC} - S_{Cl})]W} = 0.99975 \pm 0.00025 \quad (24)$$

where

$S_C$	signal measured from cavity
$S_{RC}$	signal measured on reference (perfect) cavity
$S_{Cl}$	signal measured with laser beam off
$S_W$	signal measured on white reference
$W$	reflectivity of white surface

The uncertainty is determined by the difference in the repeated measurements.

Since the tip of the cone must be withdrawn to be able to send the laser beam into the cavity, it could be that a retroreflection effect would induce some systematic error at the conclusion of the experiment. Therefore we also measured this effect by putting a semitransparent mirror in the way of the laser beam to observe an eventual retroreflection with a monitor silicon cell detector.

## THERMAL EFFECTS ON SURFACE OF SENSITIVE AREA

### Sensitive Area

The physical definition of the sensitive area of the absolute radiometer is very important because its value is one of the factors in the radiometric

equation. This area is circular and separates the radiative incident flux to be measured ( $\Phi$ ) from the flux which is to be rejected from the measurement ( $\Phi_p$ ).

The area given by its diameter should be perfectly circular; however, since this is not strictly possible, the profile as well as the departure from roundness should be known. It is a good practice to cross-check the number obtained by one metrological laboratory with that obtained independently by another. Of course this area is temperature dependent; we apply the formula

$$S_T = S_{T_0} \left[ 1 + K(T - T_0)^2 \right] \quad (25)$$

which is valid for the linear expansion of stainless steel ( $K = 11 \times 10^{-6}/^\circ\text{C}$ ). Stainless steel was chosen because it is corrosion resistant and can easily be polished. Indeed it was proven to be necessary to attenuate  $\Phi_p$  by rejecting it back through the front aperture. The surface of the sensitive area is therefore a slightly spherical mirror.

#### Thermally Induced Perturbations

Although a mirror is used, it may be that part of the absorbed  $\Phi_p$  induces a radiometric deviation; an experiment has thus been designed to measure this effect in air or vacuum conditions. The setup is identical to that for the determination of the efficiency distribution except that the mirror at the surface of the sensitive area has been replaced by one without a hole. As the effect is small the power of the laser beam used was increased to 200 mW. The laser scans the diameter of the mirror and the detector output is measured. The results, shown in figure 11, indicate a remarkable difference between air and vacuum conditions, indicating that some energy transfer occurs through convection effects.

The effect on the radiation measurement of the function  $f(\rho)$  assumed to be cylindrically symmetrical is obtained as follows: let  $\Phi = ES$  be the flux through the sensitive area  $S$ , where  $E$  is the uniform irradiance. Irradiating the whole front aperture gives rise to the thermal effects  $\Phi_T$ , whose ratio to  $\Phi$  is given by  $\tau$  such that  $\tau_i = \Phi_{T_i}/\Phi$ , where the subscript  $i = a$  (air) or  $v$  (vacuum) indicates the experimental condition. The value of  $\tau_i$  is obtained from

$$\tau_i = \frac{\int_r^R 2\pi f(\rho)\rho \, d\rho}{\int_0^R 2\pi f'(\rho)\rho \, d\rho} \quad (26)$$

where  $f(\rho)$  is the distribution of the thermal effect as a function of the location of the constant perturbation. In air this is given by

$$f(\rho) = -2.94 \times 10^{-4} \rho^2 - 2.192 \times 10^{-4} \rho + 0.11239 \quad (27)$$

where

$f'(\rho)$  is constant and equal to 200 mW

$r$  radius of the sensitive aperture

$R$  radius of the front aperture

In air, with  $R = 11.15$  mm and  $r = 4$  mm, we find that  $\tau_a = 3.045 \times 10^{-3}$ . Since  $f(\rho) = 3.02 \times 10^{-3}$  mW in a vacuum, we find for the same conditions that  $\tau_v \leq 0.1022 \times 10^{-3}$ . If the front aperture diameter is changed to a lower value, then  $\tau_a$  and  $\tau_v$  are decreased accordingly (fig. 12).

#### Sensor Emission Effects

When both channels of the absolute radiometer are closed, both sensors emit the same amount of radiation towards the closed FOV limiting device, and they also receive the same amount of energy from this assumed isothermal enclosure  $\Phi_\rho$ . However, when one of the channels is open there is a small dissymmetry in the system because the view factor towards the opened front aperture is different for the two sensors. This difference has not been taken into account because its effect is negligible.

#### EFFECT OF THE FIELD-OF-VIEW LIMITING SYSTEM

In front of the sensor, whose field of view is quite large, we have installed a removable field-of-view limiting system. Its inner surface is covered with grooves coated with black diffusing paint. The geometry of the instrument is defined by the sensitive surface and the circular front aperture diaphragm, which is centered on the sensor axis. (See the section on the angular response of the instrument.)

Among the different effects which can influence the absolute irradiance measurements are the following:

Part of the light falling on the front aperture can be scattered into the sensor's aperture. If  $\Phi_\Sigma$  is the perturbation for a given incident irradiance  $E$ , this effect is characterized by the ratio  $\Sigma' = \Phi_\Sigma/ES$  where  $s$  is the area of the sensitive surface.

Part of the light falling on the entrance aperture is dispersed on the inner part of the view-limiting device, and is absorbed. However, a certain amount,  $\Phi_\Sigma$ , can be reflected back into the sensor. The ratio  $\Sigma = \Phi_\Sigma/ES$  takes this effect into account.

Some radiation issued from the umbra zone can reach the inner wall of the view limiter, and part of it can be reflected into the sensor (fig. 13). This effect has not yet been measured. It may be very difficult to correct for this objectively because it depends specifically on the external parasitic source distribution.

Diffraction can occur on the front diaphragm as well as on the sensitive area itself; however, these effects, which are expressed by  $\delta = \Phi_{\delta}/ES$ , are negligible.

The experimental determination of these different errors is difficult because the effects are relatively small and because the laser beam has a spatial radiation distribution which is quasi-Gaussian. Therefore, the experiments had to be designed on a differential basis, using a silicon cell instead of the cavity detector to enable effective separation of the thermal effects already measured. (Refer to the section on thermal effects.)

In the first configuration (A in fig. 13) the incident beam is measured while scanning a diameter of the sensor, the front surface is coated black to avoid backscattered light, and the FOV limiter is removed. In the second configuration (B in fig. 13) the laser beam is again moved over the same diameter from one side of the front aperture to the other. The general experimental setup is shown in figure 14. The signals are subtracted from each other and the levels  $\beta$  and  $\gamma$  (fig. 15) are compared to the input signal. The results are shown in figure 15.

An analysis of the differential output function (fig. 15) suggests that the zones between WA and IJ indicate the noise level of the experiment ( $\sim 7 \times 10^{-6}$  V compared to 11.58 V). The peaks B and H indicate the objective effect of the diffraction combined with scattering on the front aperture ( $\Phi_{\Sigma} + \Phi_{\delta}$ ), the distance between B and H being exactly the front aperture diameter. The shape of the signals ABC and GHI is an image of the shape of the laser beam of about 3 mm diameter. The signal DEF suggests that the sensitivity of the silicon cell associated with the repeatability of the positioning of the laser beam is very difficult to achieve to better than 0.5 percent, due to the slope of the beam shape. Therefore, the information between C and G will not be used. The levels C and G are interpreted to be the effect due to  $\Phi_{\Sigma}$ . Therefore we have

$$\Sigma = \frac{\Phi_{\Sigma}}{ES} = \frac{\int_r^R 2\pi f(\rho)\rho d\rho}{\int_0^r 2\pi f'(\rho)\rho d\rho} \quad (28)$$

When  $r = 4$  mm,  $R = 11.15$  mm,  $f'(\rho) = 11.56$ , and  $f(\rho) = 1.28 \times 10^{-5}$ , we find that

**ORIGINAL PAGE IS  
OF POOR QUALITY**

$$\Sigma = \frac{1.28 \times 10^{-5} (11.15^2 - 4^2)}{11.56 \times 4^2} = 0.749 \times 10^{-5} \quad (29)$$

Since the effect of diffraction and dispersion is due to the edge of the front aperture,  $\Sigma' + \delta = (\Phi_{\Sigma'} + \Phi_{\delta})/ES$  should be calculated in a different way than for  $\Sigma$ . In fact, we have  $\Phi_{\Sigma'} + \Phi_{\delta} = f(R)2\pi R/\Delta$  when  $\Delta$  is the width of a rectangular laser beam of equivalent power to the actual beam. It is estimated that  $\Delta = 4.76$  mm. Thus we have for the dispersion and diffraction  $\delta$

$$(\Sigma' + \delta) = \frac{f(R)2\pi R}{\Delta \int_0^r 2\pi f'(\rho)\rho d\rho} = \frac{3.1416 \times 2 \times 11.15 \times 1.8 \times 10^{-3}}{3.1416 \times 11.156 \times 4^2 \times 1.18 \times 2} = 9.19 \times 10^{-5} \quad (30)$$

For  $R \geq r$ , this factor is a linear function of the diameter of the front aperture such that  $\Sigma' + \delta = 8.24 \times 10^{-6} R$  ( $R$  in mm).

#### LINEARITY OF THE ABSOLUTE RADIOMETER SYSTEM

It can be shown that the active radiometer servo system will work linearly when a square root function is used in its loop. If this is so, then the precision of the measurement is constant over the working range. Even if the detectors used were nonlinear, which is not the case, the measuring method based on simultaneous or successive balance measurements always gives a linear result.

#### SPECTRAL SENSITIVITY OF THE ABSOLUTE SENSOR

The measured radiative energy is given by

$$\int_{\lambda} \alpha_{\text{eff}}(\lambda) E_{\lambda} d\lambda = \frac{K}{S} (P_c - P_o) \quad (31)$$

where  $\alpha_{\text{eff}}(\lambda)$  is the sensor efficiency at wavelength  $\lambda$ . This energy is dependent on the geometry of the cavity and or its inner coating. It has been determined for one wavelength and should be extended to the whole range of wavelengths over which the observed radiation source emits energy. In fact, the solar source peaks at 460 nm, and as the black paint's absorptivity is quite constant over the solar radiation range it is reasonable to take the efficiency determined for 514 nm and use it over the whole range without appreciable error; thus

$$\int_{\lambda} E_{\lambda} d\lambda = \frac{K}{\alpha_{\text{eff}}(514)S} (P_c - P_o) \quad (32)$$

## FREQUENCY RESPONSE OF HEAT FLUX DETECTOR AND

### ABSOLUTE RADIOMETER SYSTEM

When the input flux to the radiometric system changes with time, it is necessary to know its frequency response in order to be able to reconstruct from the measurements the real-time behavior of the incident radiation. This characteristic has been determined for the heat flux detector itself as well as for the complete radiometric system (detector and feedback circuitry) to illustrate the improvement of the detector's otherwise relatively poor frequency response.

The experimental setup is shown in figure 16. It enables the determination of the transfer function in either case and is based on the equation

$$H(f) = \overline{G_{YX}(f)} / \overline{G_{XX}(f)} \quad (33)$$

where  $\overline{G_{YX}(f)}$  is the mean cross spectrum of input and output signals and  $\overline{G_{XX}(f)}$  is the mean autospectrum of the input signal. Along with the calculation of  $H(f)$ , the coherence function  $\gamma^2$  is also determined to guarantee the value found for  $H(f)$ :

$$\gamma^2 = \left[ \overline{G_{YX}(f)} \right]^2 / \overline{G_{XX}(f)} \left[ \overline{G_{YY}(f)} \right] \quad (34)$$

The radiometric excitation signal is a laser beam chopped in a pseudo-random way. It is measured by an optocoupler, and along with the radiometric output signal (with or without radiometer electronics) is filtered and sent to a Fourier analyzer.

The radiometer itself is operated in air and in a vacuum. The results show that there is no appreciable difference in behavior between air or vacuum response. This means that the thermal contacts are well settled due to the repeated and long vacuum-air cycling.

The compared responses of the detector alone (fig. 17) and the complete radiometric system with feedback (fig. 18) show, as anticipated, a remarkable improvement in the frequency response of the detector used in the system.

### RADIOMETRIC EQUATION

The radiometric equation describes the significance of the measurement. At steady state, with the Sun perfectly aligned with the radiometer axis, we have:

$$\alpha_{\text{eff}}(ES_T + \Phi_T + \Phi_\Sigma + \Phi_{\Sigma'} + \Phi_\delta + \Phi_\rho - \Phi_R - \Phi_{\rho'}) = (P_O - P_C) \left[ \frac{(R_1 + R_M)^2}{R_1 G_1 H_a H_C^2} - 1 \right] \quad (35)$$

where

$E$	irradiance ( $\text{W}/\text{m}^2$ )
$S_T$	sensitive area at temperature $T$
$\Phi_T$	thermal effect on sensor surface
$\Phi_\Sigma$	scattering due to FOV limiter
$\Phi_{\Sigma'}$	scattering on front aperture
$\Phi_\delta$	diffraction effect on aperture
$\Phi_\rho$	energy from FOV limiter when channel is open
$\Phi_{\rho'}$	energy from FOV limiter when channel is closed
$\alpha_{\text{eff}}$	efficiency of sensor
$P_C$	electrical compensation power in closed state
$P_O$	electrical compensation power in open state

with

$$(P_C - P_O) = R_1(I_{1c}^2 - I_{10}^2) + (r_c + r_d)(I_{1c}^2 - I_{10}^2) \quad (36)$$

and

$$S_T = S_{T_0} \left[ 1 + K(T - T_0)^2 \right] \quad (37)$$

Since

$$ES_T + \Phi_T + \Phi_\Sigma + \Phi_{\Sigma'} + \Phi_\delta - \Phi_R = ES_T \left[ 1 + \tau + \Sigma + \Sigma' + \delta - (1 - a_R) \right] \quad (38)$$

ORIGINAL PAGE IS  
OF POOR QUALITY

with  $ES = \Phi$  and  $\tau = \Phi_{\tau}/\Phi$ ,  $\Sigma = \Phi_{\Sigma}/\Phi$ ,  $\Sigma' = \Phi_{\Sigma'}/\Phi$ ,  $\delta = \Phi_{\delta}/\delta$ . Since at this measurement  $R_1 I_{1c}^2 = I_C V_C$  and  $R_1 I_{10}^2 = I_O V_O$ , we find that

$$E = \frac{\left[ (I_C V_C - I_O V_O) + (r_c + r_d) (I_{1c}^2 - I_{10}^2) \right] \left[ \frac{(R_1 + R_M)^2}{R_1 G_1 H_a H_c^2} - 1 \right] - \alpha_{\text{eff}} (\Phi_{\rho} - \Phi_{\rho'})}{S_{T_O} \left[ 1 + K(T - T_O)^2 \right] \left[ 1 + \tau + \Sigma + \Sigma' + \delta - (1 - a_R) \right] \alpha_{\text{eff}}}$$

(39)

REFERENCE

Kendall, J. M., Jr. 1978: Analysis and Tests of a Wide Angle Radiometer View Limiter. JPL Publication No. 78-63, Jet Propulsion Laboratory, California Institute of Technology.

## SYMBOLS

$a$	absorption coefficient
$a_R$	absorption coefficient of cavity
$a_p$	absorption coefficient of paint
$D_i$	detector
$d(z)$	relative radiation distribution function of radiative energy reflected from bottom of cavity towards wall of cylinder band
$E$	irradiance incident on sensor
$ES$	flux through sensitive area of sensor
$F$	reference voltage
$f$	frequency
$f(\rho)$	distribution of thermal effect as a function of location of perturbation
$G_i$	ratio of output signal of detector to electrical power $P_i$
$G_{XX}(f)$	mean autospectrum of input signal
$G_{YX}(f)$	mean cross spectrum of input and output signals
$H$	transfer function amplitude
$H_a(f), H_c(f)$	block transfer functions
$I_i$	heater current
$I_c$	compensation current
$K_i$	proportionality coefficient
$L$	all thermal losses except those from the sensor area itself
$L'$	all thermal losses in cavity when sensor is electrically excited
$l$	distance between front aperture plane and sensor plane
$m(z)$	relative efficiency function of tube
$P_c$	electrical compensation power (detector closed)
$P_i$	electrical power

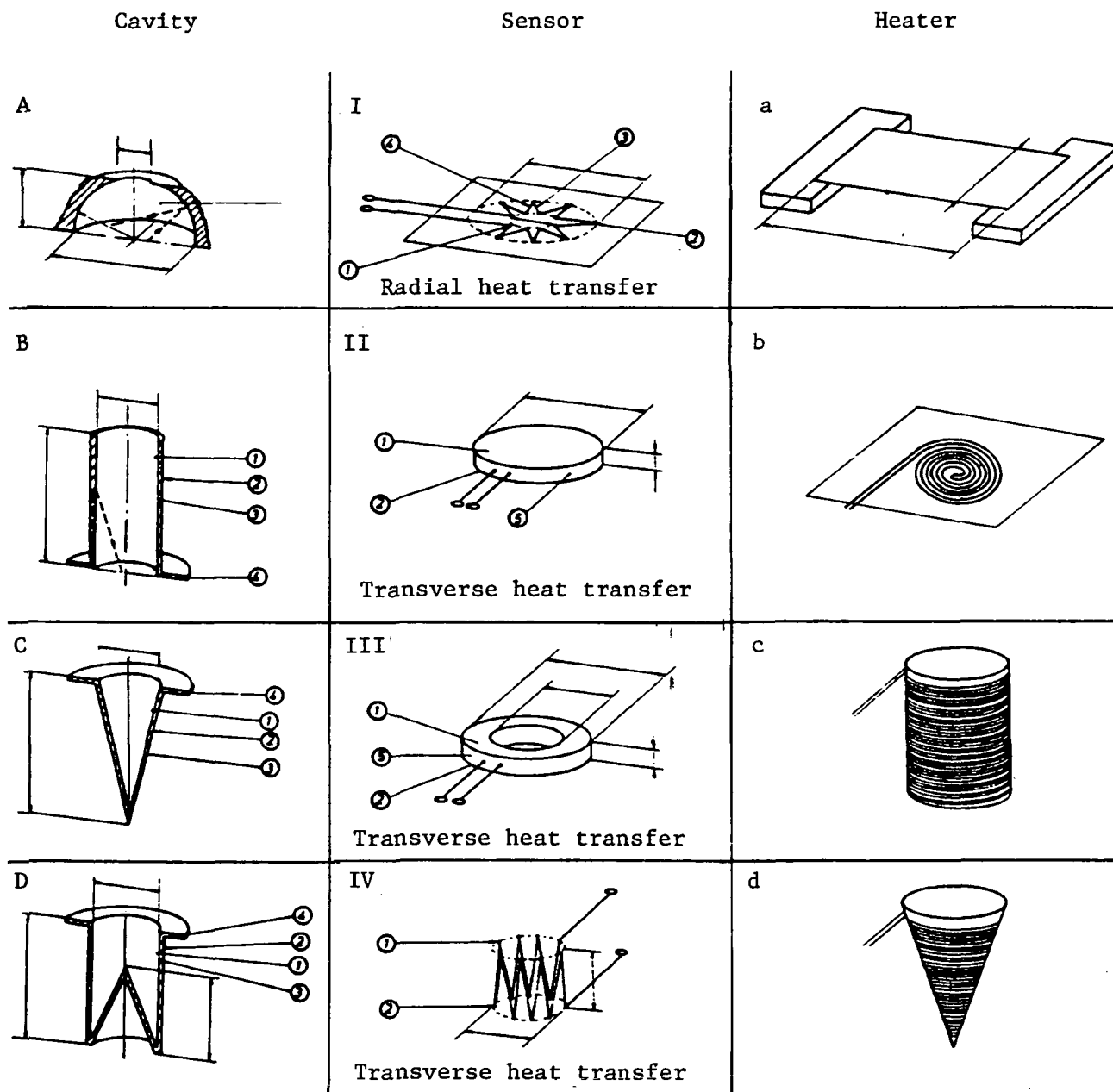
$P_o$	electrical compensation power (detector open)
$P_{pi}$	parasitic measured power
$p_1, p_2$	indices for parasitic heating effects
$R$	radius of front aperture
$R_M$	reference resistance
$R_i$	value of compensating heating resistance for detector
$r$	radius of sensor aperture
$r_i$	parasitic heaters
$S$	sensitive area of sensor
$S_{RC}$	signal measured on reference (perfect) cavity
$S_T$	sensitive area at temperature $T$
$S_{T_0}$	sensitive area at reference temperature $T_0$
$S_c$	signal measured from cavity
$S_{cl}$	signal measured with laser beam off
$S_w$	signal measured on white reference
$s$	point source
$T$	temperature
$U_i$	applied voltage
$V_{li0}$	residual thermoelectric offset
$V_{liP}$	voltage given by detector $i$ when electrically powered
$W$	reflectivity of white surface
$Z_1$	limit angle
$Z_p$	slope angle
$z$	height above bottom of cylinder
$\alpha(z)$	relative efficiency function along wall surface of cylinder
$\alpha_{eff}$	efficiency factor of sensor

$\alpha_{\text{eff}}(\lambda)$	sensor efficiency at wavelength $\lambda$
$\alpha_i$	optical efficiency of detector $D_i$
$\Delta$	width of rectangular laser beam
$\Delta V$	error signal
$\delta$	$\Phi_\delta/\Phi$
$\lambda$	wavelength
$\rho$	$\Phi_\rho/\Phi$
$\Sigma$	$\Phi_\Sigma/\Phi$
$\Sigma'$	$\Phi_{\Sigma'}/\Phi$
$\Phi$	incident radiation flux
$\Phi_E$	energy emitted by cavity
$\Phi_R$	radiation reflected by cavity
$\Phi_1$	incident radiation flux at steady state
$\Phi_P$	radiative incident flux to be rejected from measurement
$\Phi_\delta$	diffraction effect on aperture
$\Phi_\rho$	energy from FOV limiter with channel open
$\Phi_{\rho'}$	energy from FOV limiter with channel closed
$\Phi_\Sigma$	scattering due to FOV limiter
$\Phi_{\Sigma'}$	scattering on front aperture of FOV limiter
$\Phi_\tau$	thermal flux incident on separation plane of sensor but not on sensitive area
$\Phi_\psi$	front aperture heating
$\Phi'_E$	energy emitted by cavity when sensor is electrically excited
$\psi$	$\Phi_\psi/\Phi$

Subscripts:

a	air
v	vacuum



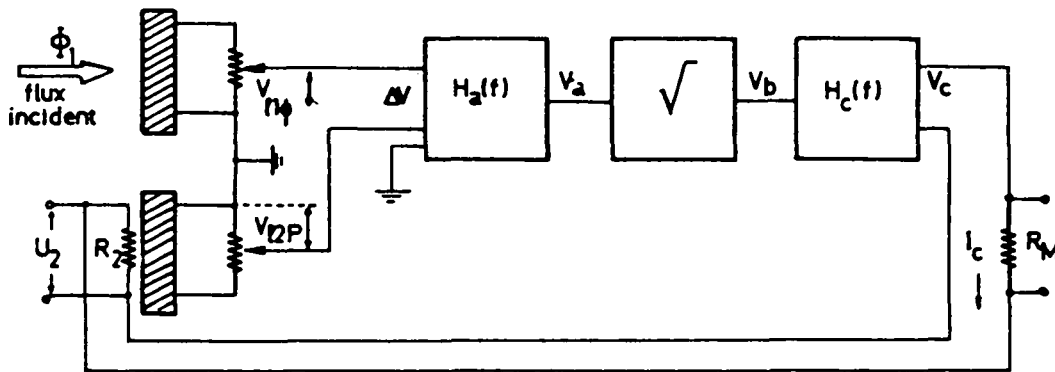


1. Absorbing surface ( $\alpha \rightarrow 1$ )
2. Reflecting surface
3. High thermal conductivity
4. Fixation ring

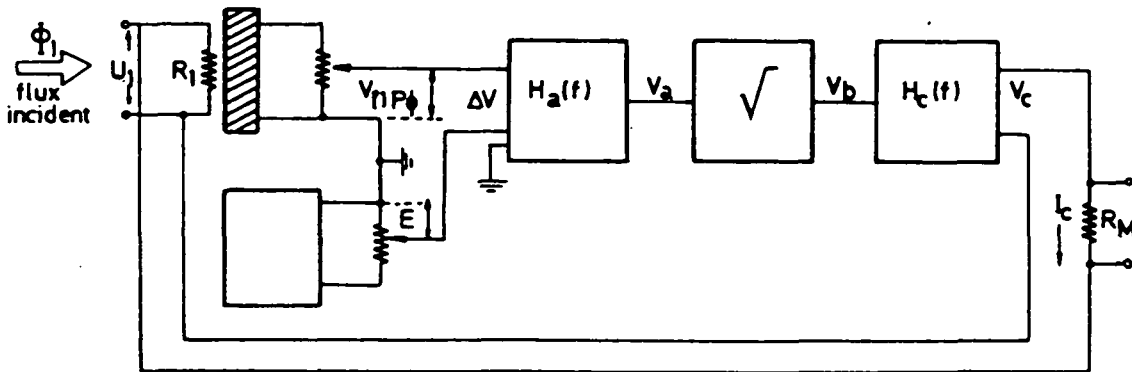
1. Hot junction
2. Cold junction
3. Type A element
4. Type B element
5. High thermal conductivity

Figure 2.- Absolute detector elements.

ORIGINAL PAGE IS  
OF POOR QUALITY



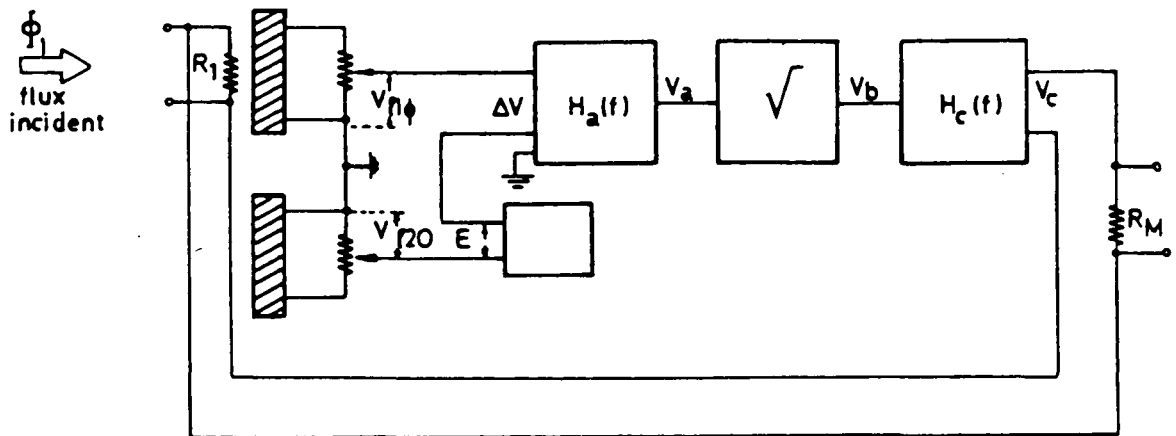
(a) Servo system for a double-compensated radiometer.



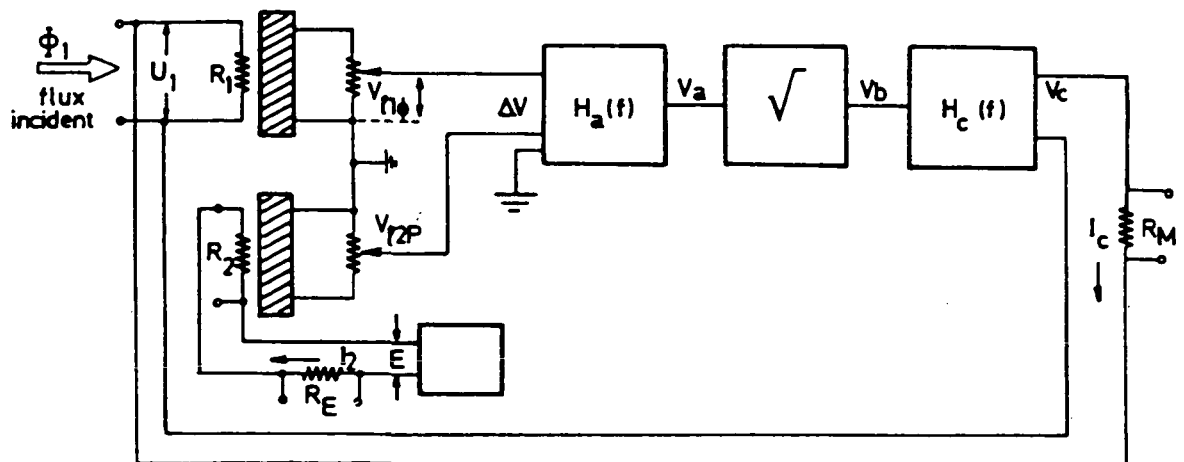
(b) Servo system for a thermally uncompensated single radiometer.

Figure 3.- Examples of radiometer servo systems.

ORIGINAL PAGE IS  
OF POOR QUALITY



(c) Servo system for a thermally compensated radiometer.



(d) Servo system for a symmetrically working compensated radiometer.

Figure 3.- Concluded.

ORIGINAL PAGE IS  
OF POOR QUALITY

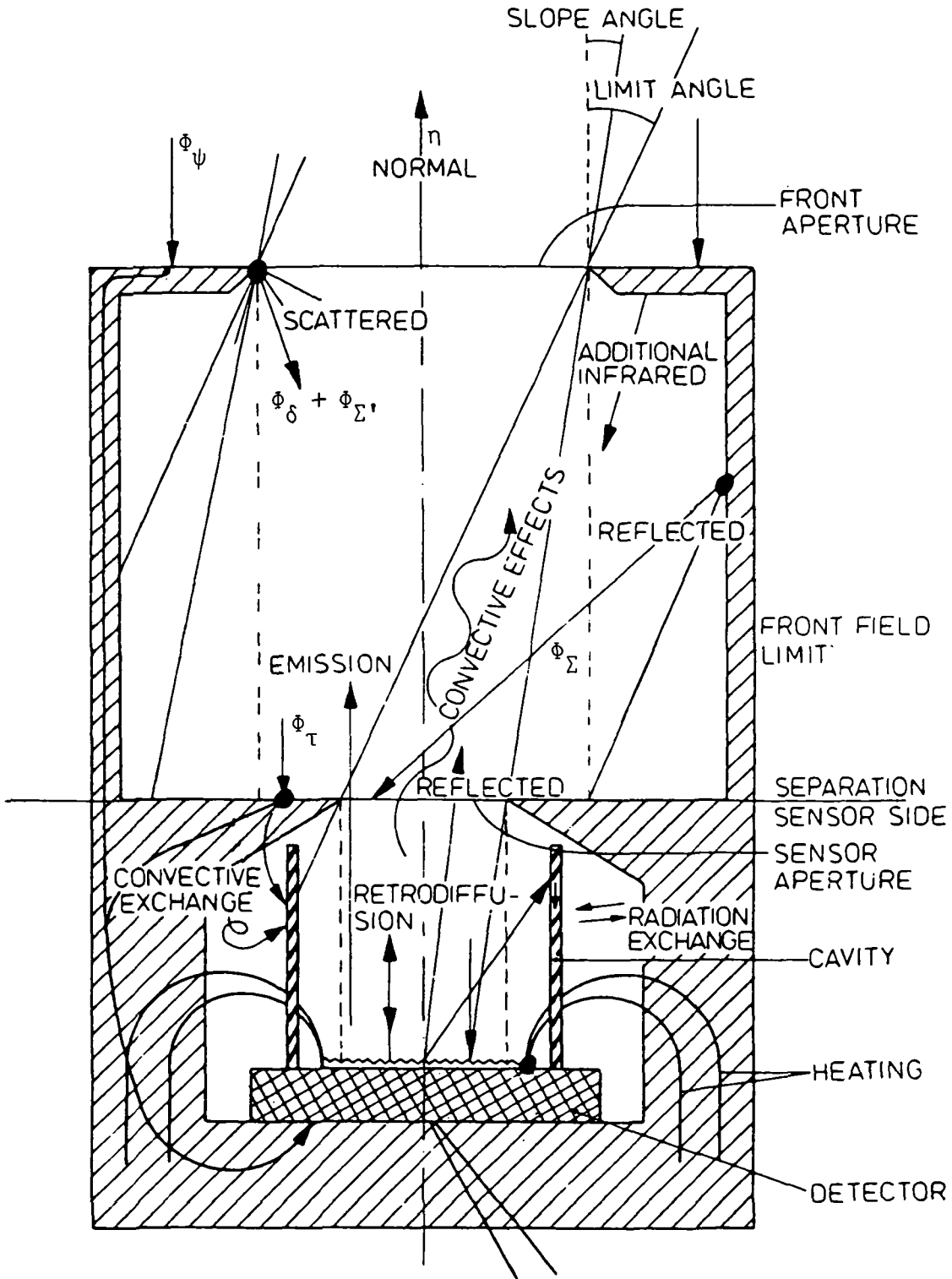


Figure 4.- Effects inducing errors on absolute radiometric measurements.

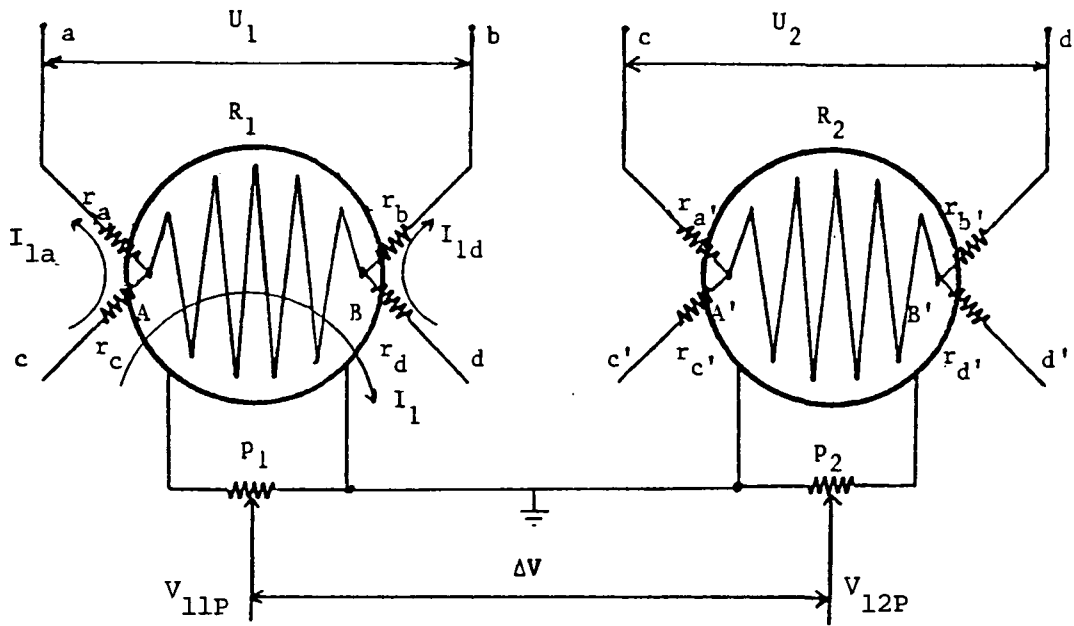


Figure 5.- Heat flux detectors and parasitic heating effect.

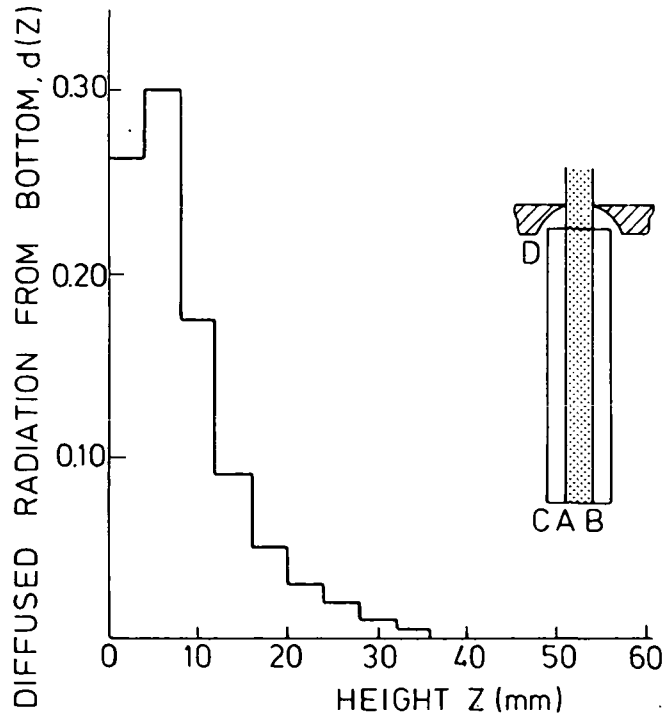


Figure 6.- Relative radiation distribution on inner wall of cavity cylinder.

ORIGINAL PAGE IS  
OF POOR QUALITY

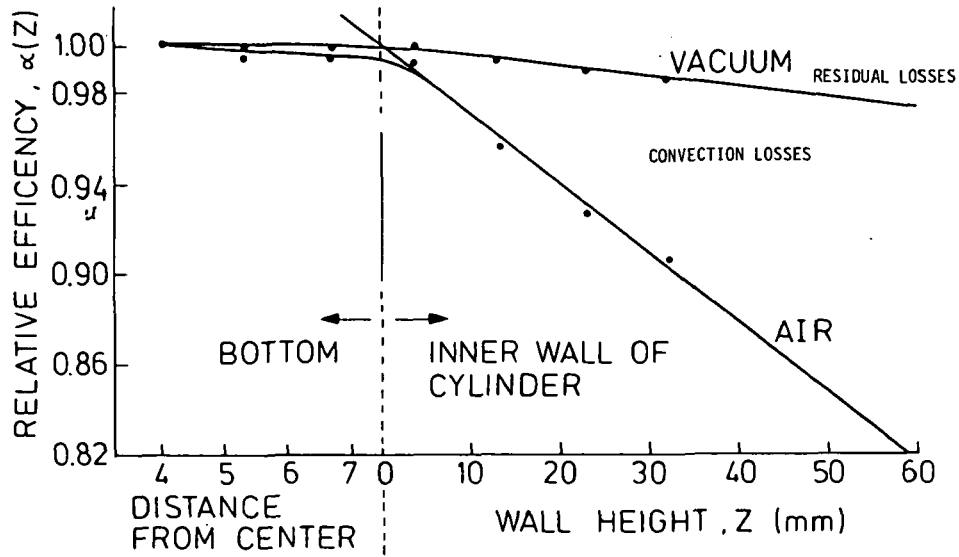


Figure 7.- Relative efficiency of cylindrical cavity  
(material: Ag, 0.5 mm thick).

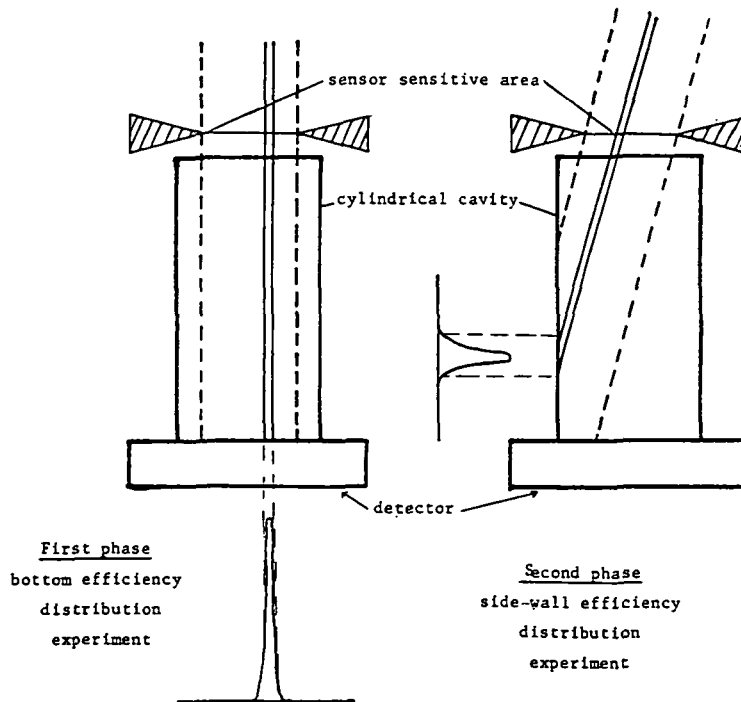


Figure 8.- Close-up of laser beam in cylindrical cavity.

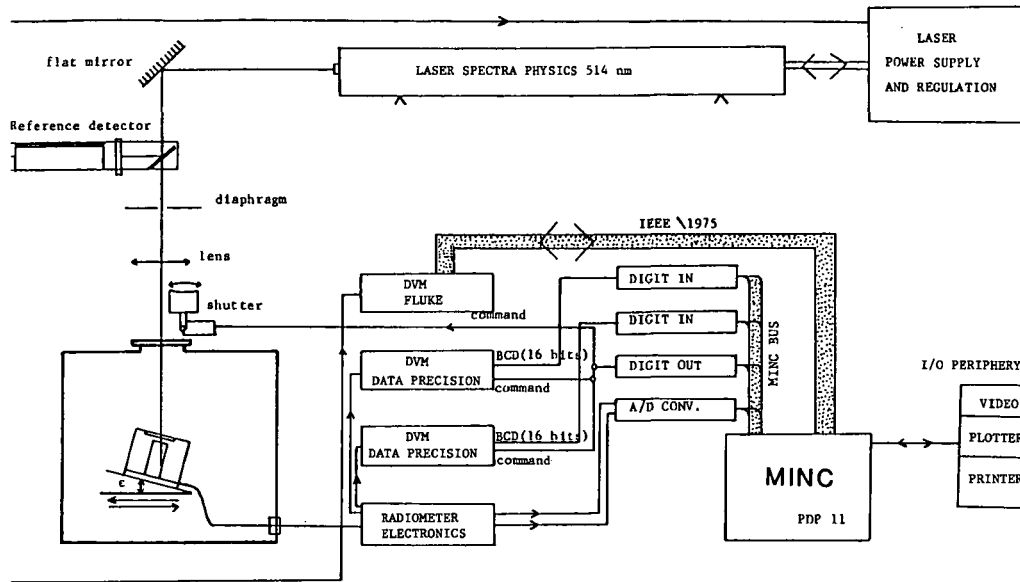


Figure 9.- Experimental setup for determination of relative efficiency distribution in radiometric cavity.

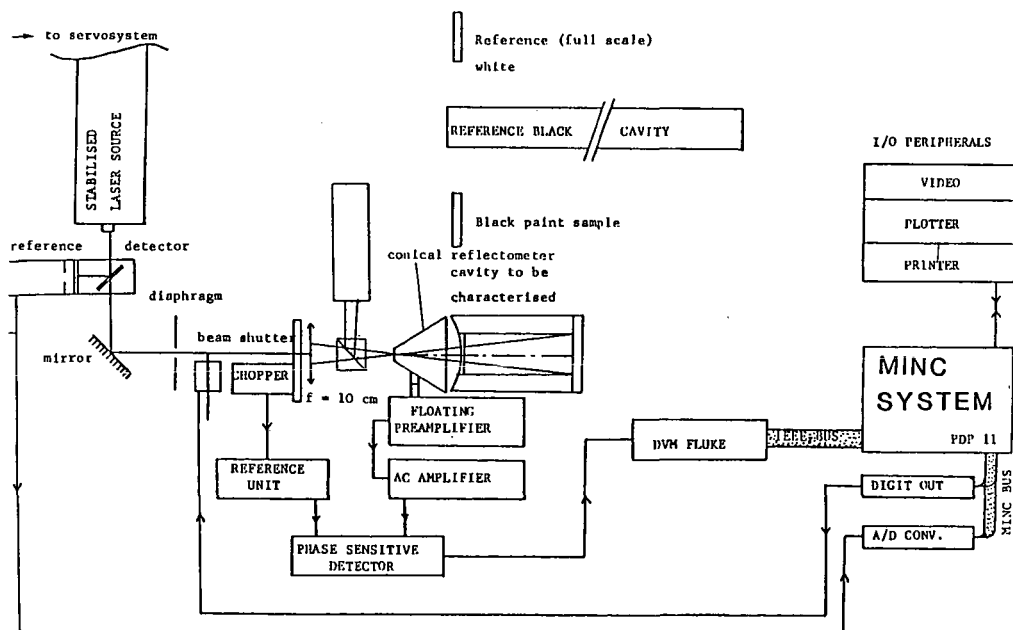


Figure 10.- Experimental setup for measurement of effective absorption coefficient and retroreflection of a cavity.

ORIGINAL PAGE IS  
OF POOR QUALITY.

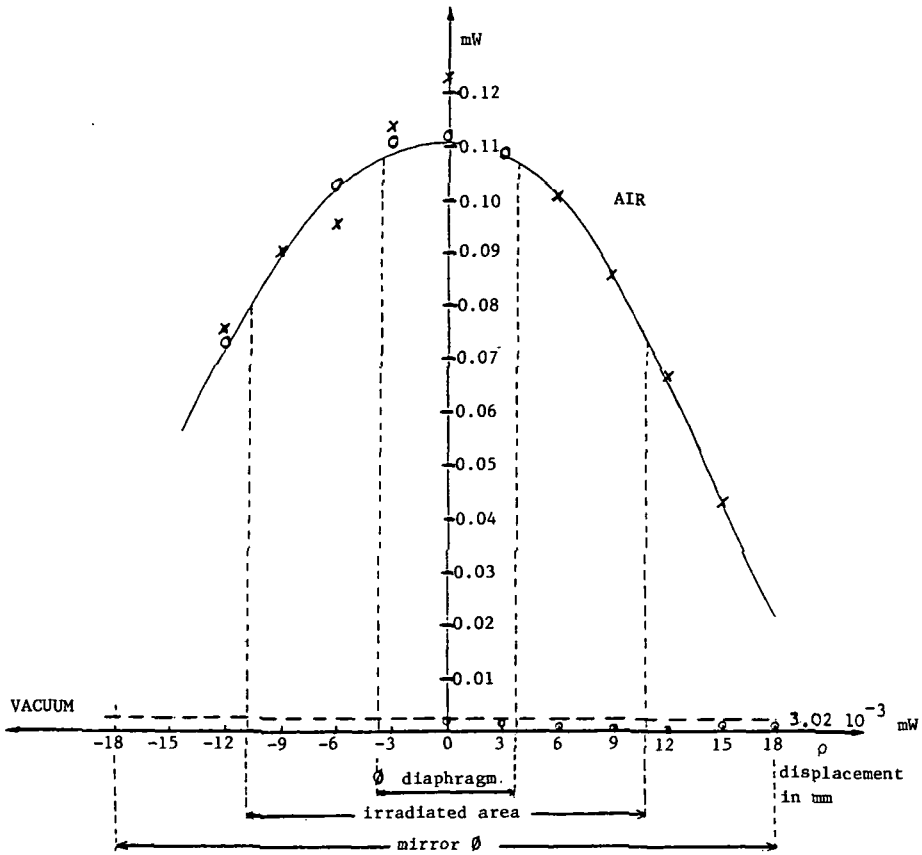


Figure 11.- Function  $f(\rho)$  measured for incident power of 200-mW laser beam. The experiment shows that  $f(\rho) = -2.94 \times 10^{-4} \rho^2 - 2.192 \times 10^{-4} \rho + 0.11239$ .

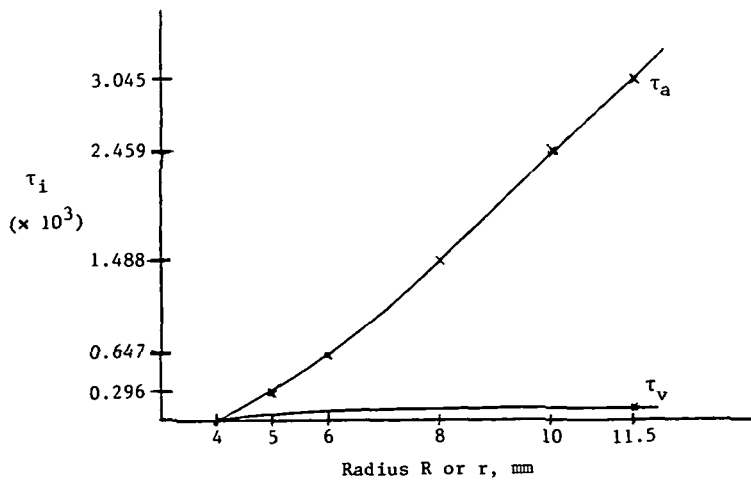


Figure 12.- Parameters  $\tau_a$  and  $\tau_v$  as a function of front aperture diameter.

ORIGINAL PAGE IS  
OF POOR QUALITY

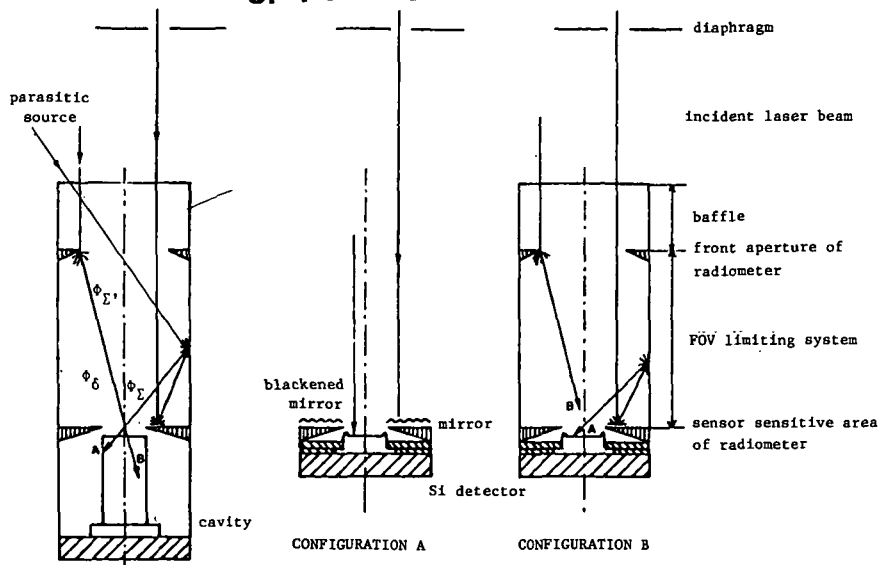


Figure 13.- Illustration of effects due to FOV limiting system. Two configurations are shown for the experiment.

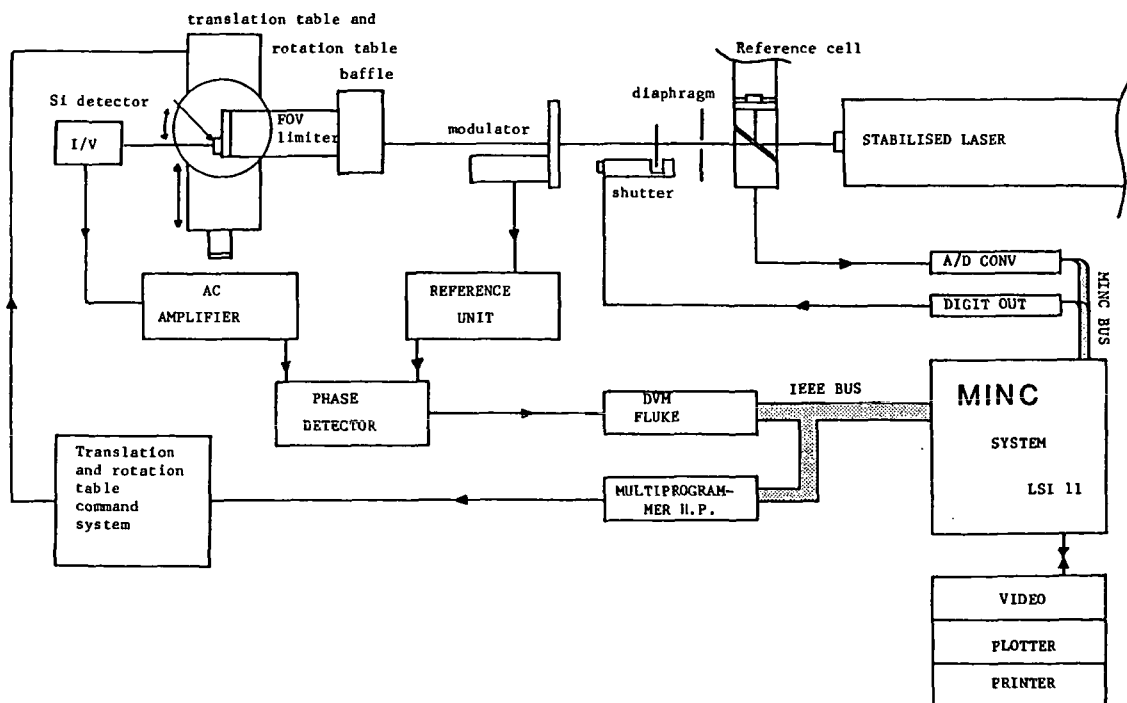


Figure 14.- Experimental setup for determination of FOV limiting system effects.

ORIGINAL PAGE IS  
OF POOR QUALITY.

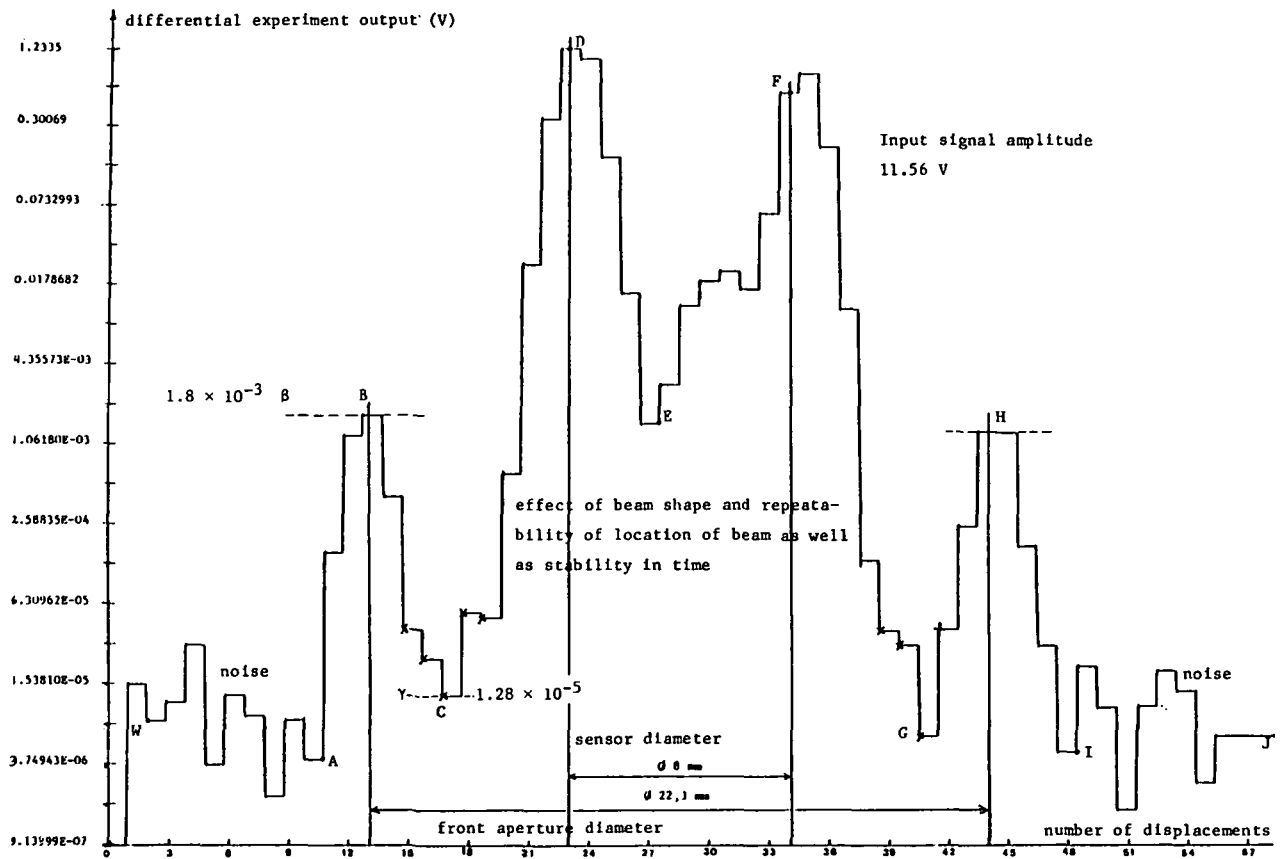


Figure 15.- Experimental result of setup shown in figure 14.

ORIGINAL PAGE IS  
OF POOR QUALITY

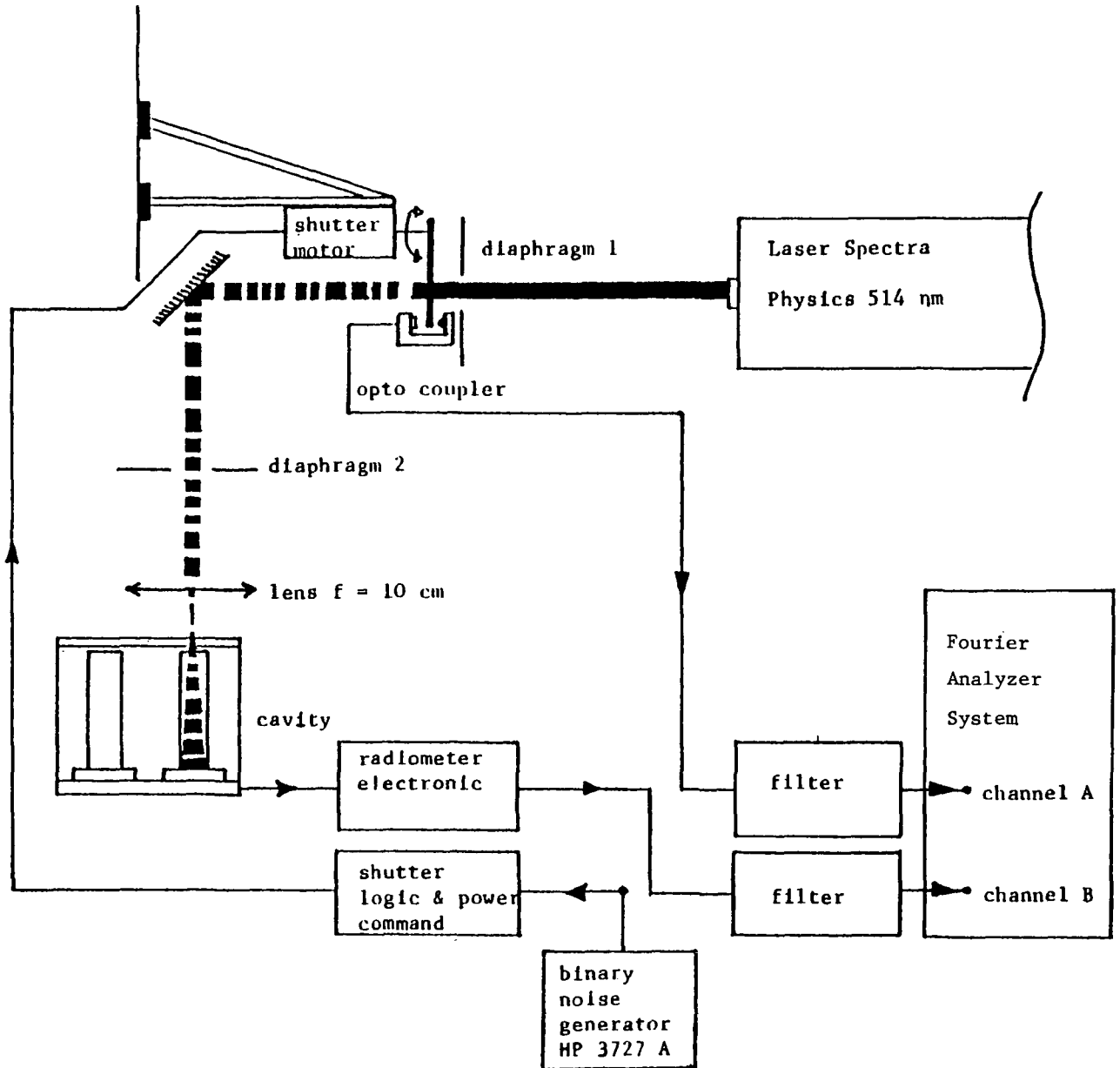


Figure 16.- Determination of transfer function of radiometer.

ORIGINAL PAGE IS  
OF POOR QUALITY

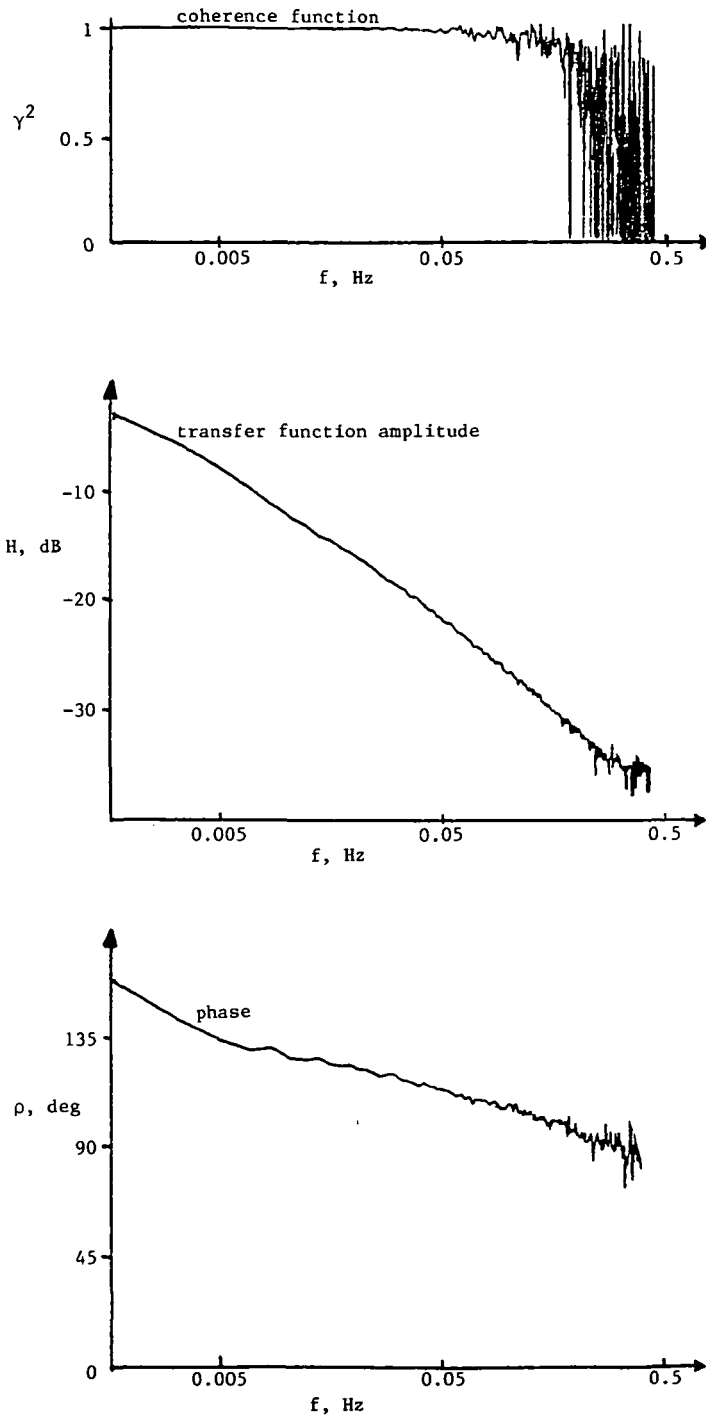


Figure 17.- Coherence and transfer functions of radiometer detector without servo system.

ORIGINAL PAGE IS  
OF POOR QUALITY

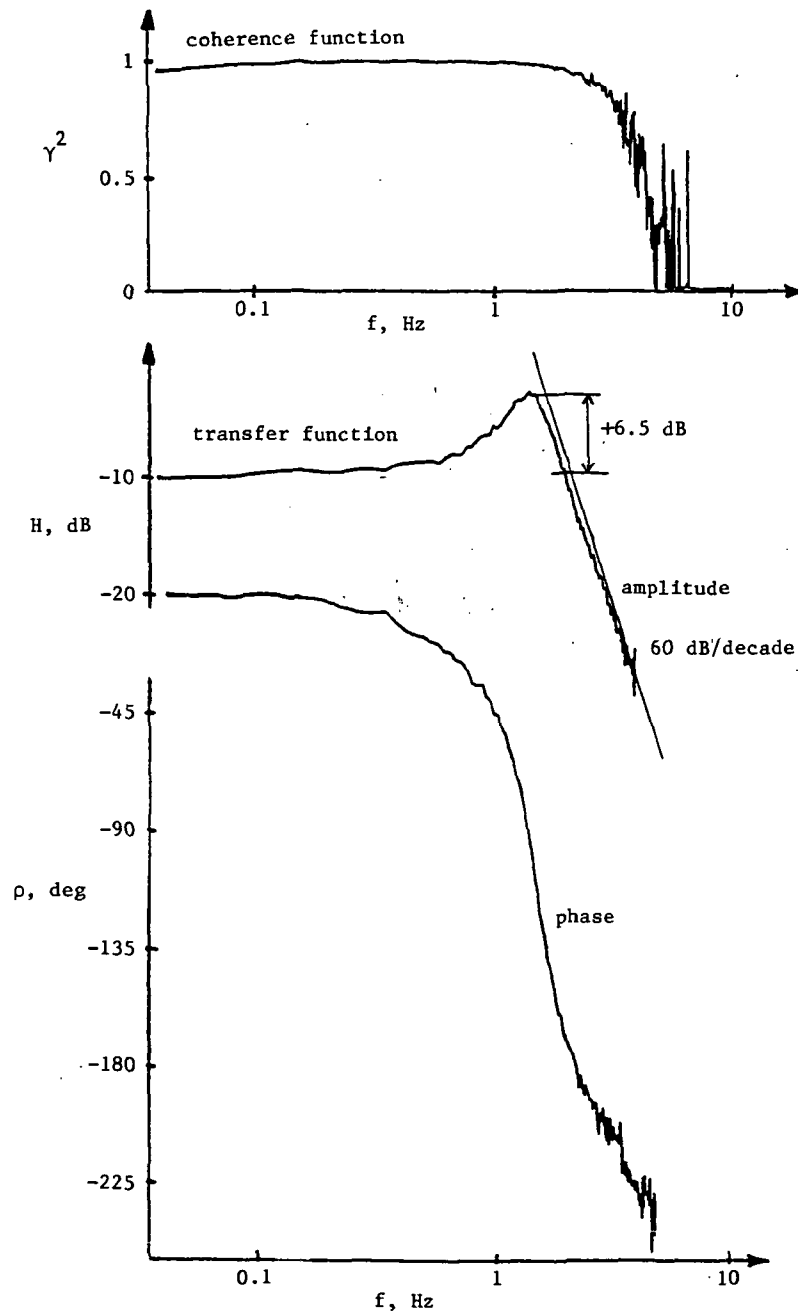


Figure 18.- Coherence and transfer functions of radiometric detector with servo system.